Article

Discrete Element Study of Particle Size Distribution Shape Governing Critical State Behavior of Granular Material

Mingdong Jiang [1,2], Daniel Barreto [3], Zhi Ding [1,*] and Kaifang Yang [1,2,*]

[1] Department of Civil Engineering, Hangzhou City University, Hangzhou 310015, China; jiangmd@hzcu.edu.cn
[2] College of Civil Engineering and Architecture, Zhejiang University, Hangzhou 310058, China
[3] School of Computing, Engineering and the Built Environment, Edinburgh Napier University, Edinburgh EH10 5DT, UK; d.barreto@napier.ac.uk
[*] Correspondence: dingz@hzcu.edu.cn (Z.D.); yangkf@hzcu.edu.cn (K.Y.)

Abstract: Granular soil is a porous medium composed of particles with different sizes and self-similar structures, exhibiting fractal characteristics. It is well established that variations in these fractal properties, such as particle size distribution (PSD), significantly influence the mechanical behavior of the soil. In this paper, a three-dimensional (3D) Discrete Element Method (DEM) is applied to study the mechanical and critical-state behavior of the idealized granular assemblages, in which various PSD shape parameters are considered, including the coefficient of uniformity (C_u), the coefficient of curvature (C_c), and the coefficient of size span (C_s). In addition, the same PSDs but with different mean particle sizes (D_{50}) are also employed in the numerical simulations to examine the particle size effect on the mechanical behavior of the granular media. Numerical triaxial tests are carried out by imposing axial compression under constant mean effective pressure conditions. A unique critical-state stress ratio in p'-q space is observed, indicating that the critical friction angle is independent of the shape of the PSD. However, in the e-p' plane, the critical state line (CSL) shifts downward and rotates counterclockwise, as the grading becomes more widely distributed, i.e., the increasing coefficient of span (C_s). Additionally, a decrease in the coefficient of curvature (C_c) would also move the CSL downward but with negligible rotation. However, it is found that the variations in the mean particle size (D_{50}) and coefficient of uniformity (C_u) do not affect the position of the CSL in the e-p' plane. The numerical findings may shed some light on the development of constitutive models of sand that undergo variations in the grading due to crushing and erosion, and address fractal problems related to micro-mechanics in soils.

Keywords: particle size distribution; granular material; discrete element method; critical state theory

1. Introduction

The particle size distribution (PSD) refers to different particle size fractions within granular material. It is well established that these fractions are fundamental in determining the texture of the material and are a key characteristic of granular soils. The distribution of these fractions significantly influences fundamental properties such as compaction, permeability, shear strength, and consolidation. Therefore, a comprehensive understanding of particle size distribution is essential for accurately predicting the behavior of granular soils in engineering applications. Recently, research on the effects of PSD has gained traction, particularly in the areas of particle breakage [1–3] and gap-graded assemblies [4,5].

Fractal theory has been widely used in describing and studying the particle size distribution (PSD) of granular material [6–10]. However, in geotechnical engineering, the wide particle size range of granular materials, such as sand and gravel, makes fractal representation challenging. Therefore, a more in-depth study of the influence of the PSD shape is necessary. Among the various PSD descriptors, the coefficient of uniformity (C_u) has been the most widely used to characterize the PSD shape [11–15]. However, since this parameter is relatively simple, it may not fully capture the complexities of PSD characteristics. As a result, other parameters, such as the coefficient of curvature (C_c) [16–18] and the coefficient of size span C_s [19], have started to receive more attention. Note, however, that these parameters are defined as a function of individual diameters (e.g., D_{10}, D_{30}, D_{50}, and D_{60}); hence, they may not always describe fully a given PSD. A more detailed investigation of these additional PSD shape descriptors is nevertheless warranted.

Critical state theory (CST), first formulated by Roscoe et al. [20], serves as the foundation for soil constitutive models. It describes an asymptotic state in which the ratio of the shear stress q to mean effective stress p' and the volume reach a steady condition during further shearing. Numerous studies on particle breakage, e.g., [21–23], have shown that the critical state locus shifts as the PSD changes. Although the shear strength at the critical state appears to be unaffected by the coefficient of uniformity C_u [24,25], Li et al. [26] found that, for a broader range of C_u, deviations in the shear strength can occur. Furthermore, as the PSD widens, the critical state locus in the *e-p'* plane initially shifts downward and may later move back upward [27–29]. This raises the following question: how does the PSD influence the critical state shear strength and the location of the critical state line (CSL) in the *e-p'* plane?

While most studies have focused on the effect of C_u on the mechanical behavior of granular materials, other PSD shape descriptors have received limited attention. The objective of this study is to analyze the impact of four PSD descriptors—mean particle size D_{50}, coefficient of uniformity C_u, coefficient of curvature C_c, and coefficient of size span C_s—on the shear and critical state behaviors of granular materials. These descriptors are defined in Equations (1)–(3):

$$C_u = \frac{D_{60}}{D_{10}} \tag{1}$$

$$C_c = \frac{D_{30}{}^2}{D_{10}D_{60}} \tag{2}$$

$$C_s = \frac{D_{100} - D_0}{D_{100} + D_0} \tag{3}$$

where D_{100} is the maximum particle diameter, D_0 is the minimum particle diameter, D_{10} is the 10% cumulative passing particle diameter, and D_{60} is the 60% cumulative passing particle diameter.

To investigate these effects, the Discrete Element Method (DEM) [30], a powerful and efficient tool for studying granular materials, is employed. The DEM allows for isolating the effects of the PSD while minimizing the influence of other variables, such as the particle shape. Seven distinct PSDs are carefully constructed to isolate the influence of each shape descriptor. The results show that, although the evolution of deviatoric stress varies with different PSDs, the ultimate shear strength remains invariant across all PSD descriptors. Moreover, an increase in the size span C_s and a decrease in the coefficient of curvature C_c tend to shift the CSL downward in the *e-logp'* plane. However, the position of the CSL in the *e-logp'* plane is not significantly influenced by PSDs with particle size scaling alone or PSDs with varying C_u.

2. Critical State Framework and Simulation Details

2.1. Critical State Framework

The critical state theory (CST) proposed by Roscoe et al. [20] is a milestone in soil mechanics and has fundamentally shaped the field [31]. The critical state (CS) refers to the ultimate state for particulate materials, in which the material continues to deform in shear at a constant volume and under constant stresses. Mathematically, the critical state can be expressed as follows:

$$\dot{p} = 0, \dot{q} = 0, \dot{\varepsilon}_v = 0 \text{ but } \dot{\varepsilon}_q \neq 0 \tag{4}$$

where p is the mean effective normal stress, q is the deviatoric stress, ε_v is the volumetric strain, and ε_q is the deviatoric strain. The over-dot notation indicates the rate of change in each quantity.

Two sufficient and necessary conditions for the critical state were defined as follows:

$$\eta = \eta_c (q/p)_c = M, \ e = e_c = \hat{e}_c(p) \tag{5}$$

where η is the stress ratio, M is the critical state stress ratio, and e_c is the critical state void ratio, which is only related to p, resulting in a unique critical state line (CSL) in the e- space. The first part of Equation (5) defines a straight line in the p-q space, which is termed the critical state line in the p-q space. The slope M of this line is an intrinsic material constant, which is also a function of the stress Lode angle.

Although both conditions in Equation (5) must be simultaneously satisfied for critical state failure, they can be independently reached. Li and Dafalias [32] revisited this theory from the thermodynamics perspective and proposed an anisotropic critical state theory (ACST) to address the limitations of the CST.

In the context of a discrete system with N_f particles, the fabric of the system can be defined by the deviatoric tensor **F**, as follows [33,34]:

$$\mathbf{F} = \frac{1}{N_f} \sum_{\alpha=1}^{N_f} n^\alpha \otimes n^\alpha - \frac{1}{3}\mathbf{I} \tag{6}$$

where **I** is the identity tensor, and $\mathbf{n}^\alpha$ represents a characteristic orientation of the discrete system, which could include void vectors [35], particle orientations [36], or contact unit normals [37]. As further explained by Li and Dafalias [38], the fabric tensor must be thermodynamically consistent with the dissipation mechanism and thus should be a per-unit volume measure. To account for the relative orientation between the fabric anisotropy and loading directions, a fabric anisotropy variable (FVA), denoted as A, is introduced:

$$A = \mathbf{F} : \mathbf{n} = F\mathbf{n}_F : \boldsymbol{n} = FN \tag{7}$$

where **n** is the deviatoric unit loading direction. The fabric tensor **F** has two non-trivial invariants: the norm F and the Lode angle θ_F, associated with the unit direction of **F**, denoted as $\mathbf{n}_F$. The Lode angle θ_F is $0°$ for triaxial compression and $60°$ for triaxial extension. The scalar N represents the product of $\mathbf{n}_F$ and **n**, signifying the relative orientation between the loading and fabric directions. The additional condition of the fabric anisotropy at the critical state can be expressed as $A = A_c = 1$. This condition implies that, during plastic deformation, the fabric evolves such that its norm gradually approaches a critical value and its direction aligns with the loading direction. The necessary and sufficient conditions for the critical state can therefore be written as

$$\eta = \eta_c (q/p)_c = M, \ e = e_c = \hat{e}_c(p), A = A_c = 1 \tag{8}$$

In this paper, the effect of four PSD shape descriptors is investigated under the anisotropic critical state framework. The contact-normal-based fabric tensor, which has been widely shown to efficiently reveal insights into sand behavior [39–41], is adopted to describe the internal fabric in this study.

2.2. Simulation Details

The open-source program YADE, developed by Kozicki and Donzé [42], is used to perform 3D Discrete Element Method (DEM) simulations in this study. The periodic boundary condition is applied to a cubic packing composed of unbreakable spheres. The cubic specimens, consisting of over 5000 particles, are considered as a representative volume element. All the particles within the cell move according to the specified strain increment $\Delta \varepsilon_{ij}$, as shown in Equation (9) [43]:

$$\Delta x_i = \Delta \varepsilon_{ij} x_j \Delta t \tag{9}$$

where Δx_i is the displacement of particle *i*, and Δt is the time step.

During the consolidation (isotropic compression) and shearing phases, an unbalanced force ratio below 0.001 was defined to ensure initial equilibrium after consolidation and quasi-static conditions during shear. Gravity is set to zero throughout all phases of the simulation. In the quasi-static state with zero gravity, increasing the particle density accelerates the simulation without affecting the accuracy of the results. To achieve this, all particles are assigned a solid density of $\rho = 2650 \times 10^3$ kg/m^3, which is 1000 times the usual density. Additionally, a default numerical damping coefficient $\xi = 0.7$ is introduced to dissipate the kinetic energy of the particles, thereby accelerating the simulation and reducing the computational costs. A parallel sensitivity study indicated that using lower values of damping did not affect the simulation results.

A linear contact law is employed, and the particle's normal stiffness is set to equal to the tangential stiffness, $k = 10^8$ N/m. Initially, spheres with the desired number of particles are generated without contact. The cubic sample is then compressed isotropically to the target pressure of 100 kPa, 200 kPa, 500 kPa, 1000 kPa, and 1500 kPa. Before shearing, the coefficient of friction between particles is set to 0.5. Subsequently, the samples are sheared to larger axial strains, at which point, the critical state can be reached.

The servo mechanism for strain rate loading, developed on the basis of the method of Thornton and Zhang [44], follows the general form of

$$\dot{\varepsilon} = G(\sigma_t - \sigma_c) \tag{10}$$

where *G* is the gain parameter, determined through trial and error, σ_t is the target stress, and σ_c is the current stress. The mean effective stress is kept constant during the triaxial shearing process.

In this study, four PSD descriptors (D_{50}, C_u, C_c, and C_s,) are investigated. The seven curves are intentionally designed to isolate the effect of each descriptor, as shown in Figure 1. On the basis of the definitions of these descriptors, it is clear that they are related to particle sizes D_0, D_{10}, D_{30}, D_{50}, D_{60}, and D_{100}. Therefore, in the PSD design, changes in these specific particle sizes were considered. Additionally, D_{90} is also included in the analysis. To begin with, four PSDs (PSD1 to PSD4) are designed, all having the same D_{50} but differing in their maximum and minimum particle sizes. Next, PSD5 is selected through trial and error, using the above nine particle sizes corresponding to different cumulative percentages, ensuring that PSD5 differs from PSD2 only by C_s and from PSD3 only by C_u. For the effect of D_{50}, a mono-sized PSD is chosen as a control. To further investigate this effect, another mono-sized PSD with a larger D_{50} is generated and named PSD6. A

similar method is used to generate PSD7 based on PSD4 in order to study the role of C_c. This design approach allows for the separate evaluation of the influences of C_s, C_u, C_c, and D_{50} on the behavior of the granular material. The details of the PSD descriptors are summarized in Table 1.
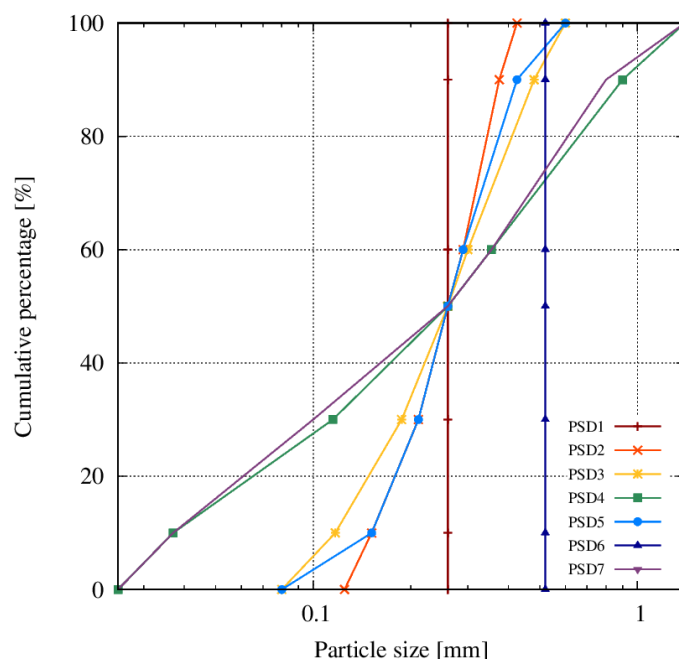
Figure 1. Particle size distribution of samples.

**Table 1.** Descriptors of particle size distribution.

| PSD Type	D_{50} (mm)	C_u	C_c	C_s
PSD1	0.26	1.000	1.000	0
PSD2	0.26	1.914	1.013	0.545
PSD3	0.26	2.564	1.002	0.765
PSD4	0.26	9.595	1.007	0.965
PSD5	0.26	1.914	1.013	0.765
PSD6	0.52	1.000	1.000	0
PSD7	0.26	9.595	0.761	0.965

3. Results

3.1. Typical Macroscopic Responses

The shear strength evolution of a group of samples with seven different PSDs (with $p_0' = 500$ kPa) under a constant mean effective stress path is presented in Figure 2. It is evident that the pace of deviatoric stress evolution varies across the different PSDs during the early stages of shearing ($\varepsilon_a \leq 10\%$). However, with further shearing, all specimens eventually reach the same shear strength.

To better understand the impact of the various PSD descriptors on the deviatoric stress evolution, these curves are grouped into four categories in Figure 3. From these plots, it is clear that the coefficient of uniformity (C_u) has almost no effect on the deviatoric stress evolution, as the curves for C_u (represented by the yellow and blue lines in Figure 3b) almost overlap from the initial shearing state to the critical state.
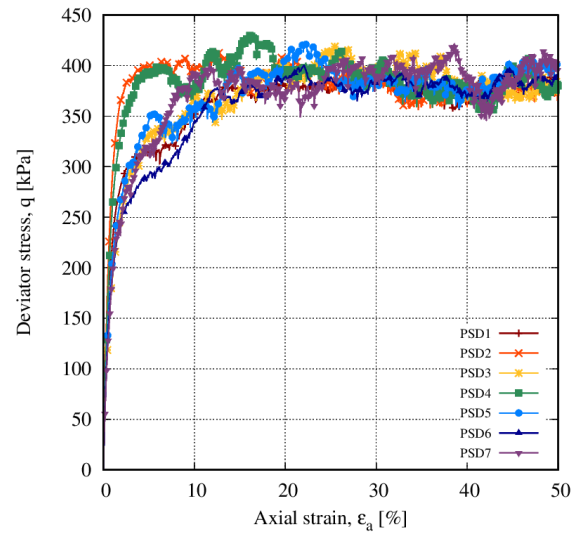
Figure 2. Deviatoric stress evolution of samples with various PSDs at $p_0' = 500$ kPa.
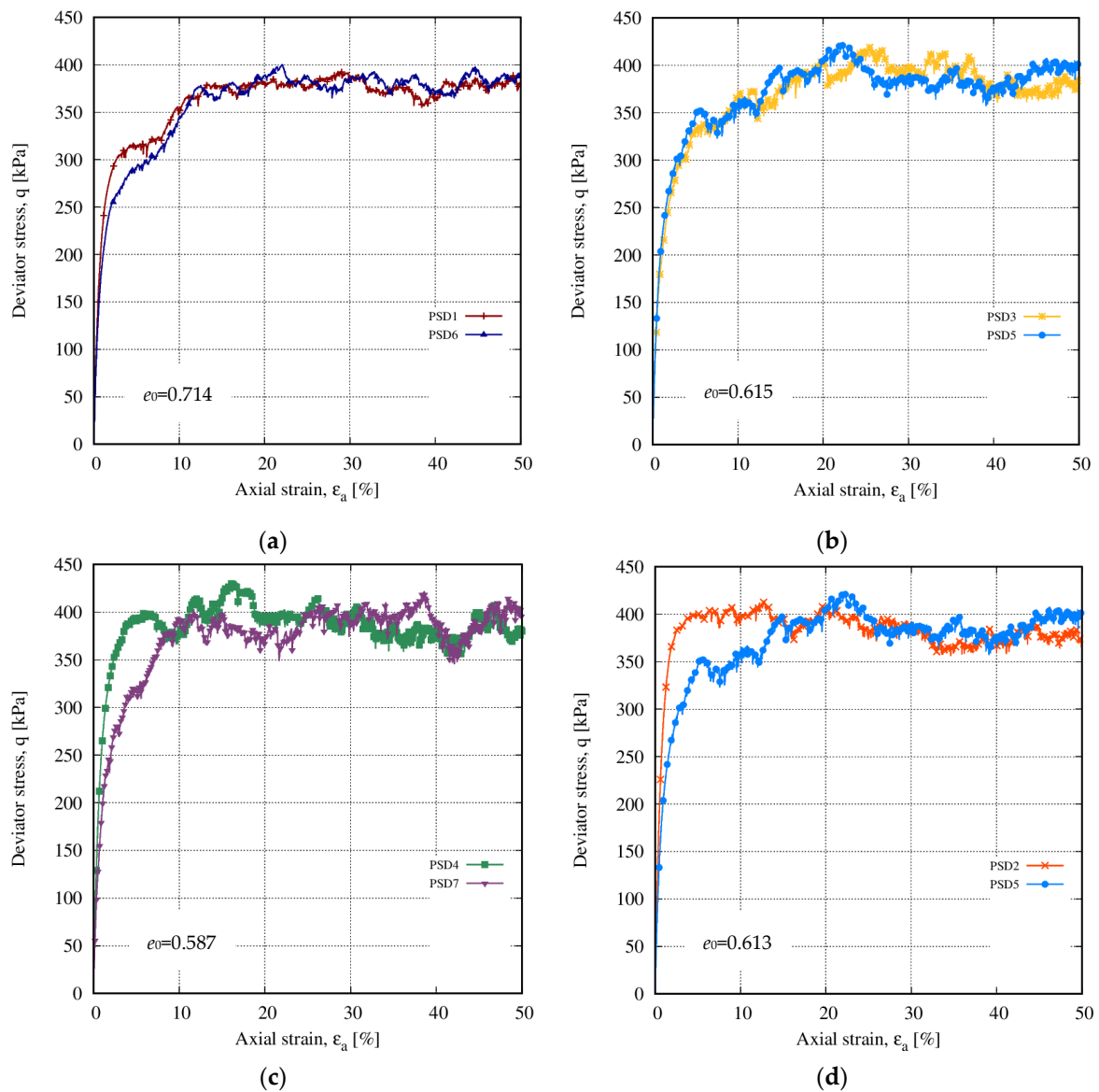

Figure 3. Effect of descriptors on deviatoric stress responses: (**a**) D_{50} effect; (**b**) C_u effect; (**c**) C_c effect; (**d**) C_s effect.

On the other hand, the mean particle size (D_{50}) appears to have a slight effect on the evolution rate of the deviatoric stress, as shown in Figure 3a. However, the overall impact of these two descriptors (C_u and D_{50}) is relatively limited.

In contrast, the deviatoric stress evolution rate is significantly influenced by the other two descriptors: the coefficient of curvature (C_c) and the coefficient of size span (C_s). Specifically, samples with a larger C_c and smaller C_s exhibit higher stiffness and higher peak deviatoric stresses. This indicates that both C_c and C_s play a more pronounced role in controlling the shear strength behavior compared to C_u and D_{50}.

The volumetric strain responses are shown in Figure 4. The samples with PSD4 and PSD2 exhibit slightly dilative behavior before reaching the critical state, consistent with previous observations of strain-softening responses. In contrast, the other five samples display volumetric contraction.
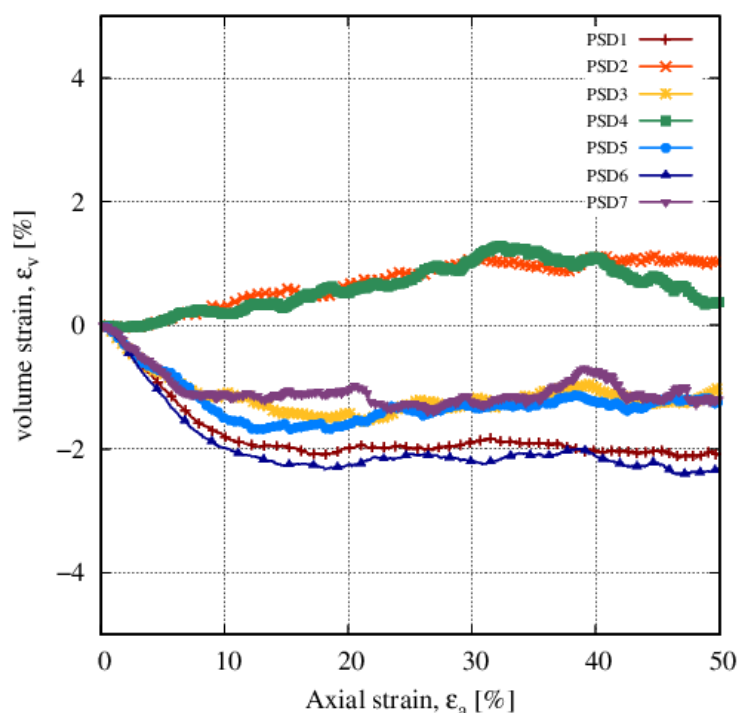

Figure 4. Volumetric responses with various PSDs at $p_0' = 500$ kPa.

To better understand the impact of different PSD descriptors on volume evolution, the results are grouped into four categories in Figure 5. For each group, despite having the same initial void ratios, the volumetric response influenced by the four PSD shape descriptors varies. Figure 5a demonstrates that all samples exhibit the same tendency of volumetric contraction until the critical state is reached, with negligible differences in volumetric strain. This suggests that the mean particle size (D_{50}) has little effect on both the volume evolution and the critical state void ratio.

Figure 5b shows that the coefficient of uniformity (C_u) has no influence on the critical state void ratio or the volumetric evolution throughout the shearing process. In contrast, the coefficient of curvature (C_c) and the coefficient of size span (C_s) significantly affect the volumetric response, as shown in Figure 5c,d. Specimens with PSD4 and PSD2 exhibit dilative behavior during shearing, while specimens with PSD7 and PSD5 experience volumetric contraction.
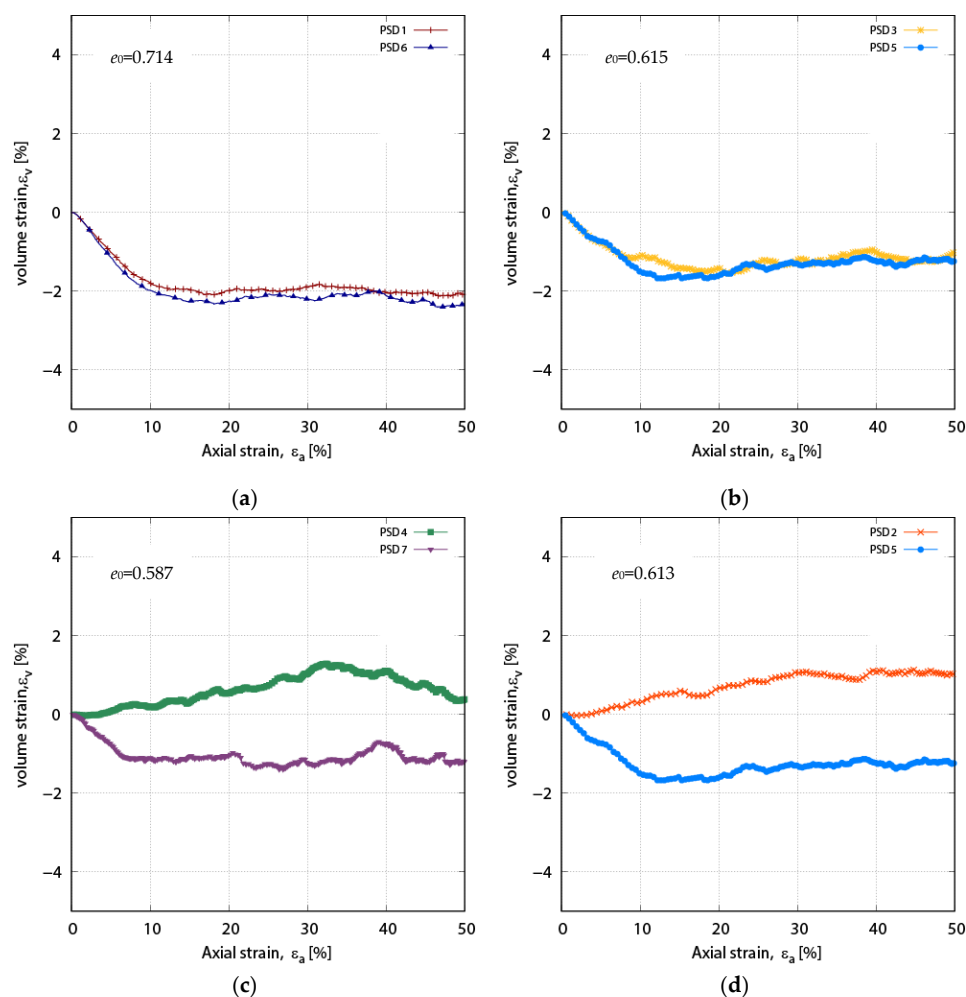
Figure 5. Effect of descriptors on volumetric responses: (**a**) D_{50} effect; (**b**) C_u effect; (**c**) C_c effect; (**d**) C_s effect.

3.2. Typical Microscopic Responses

The coordination number (Z_m) serves as a scalar measure of the contact features in granular materials. Defined as the ratio of twice the number of contacts to the number of particles, it quantifies the average number of contacts per particle and provides critical insights into the microstructural evolution of the material. The mathematical expression for Z_m is as follows:

$$Z_m = 2\frac{N_c - N_p^1}{N_p - \left(N_p^1 + N_p^0\right)} \tag{11}$$

Here, N_p and N_c represent the total numbers of particles and contacts, respectively. N_p^1 and N_p^0 are the numbers of particles with only one contact and no contacts, respectively. This definition excludes particles with fewer than two contacts, as they do not contribute to stress transmission.

Figure 6 shows the evolution of Z_m with axial strain. Consistent with findings from previous DEM studies, Z_m decreases with increasing axial strain. The influence of PSD descriptors on the Z_m evolution is illustrated in Figure 7. Similarly to the macroscopic responses, D_{50} and C_u exhibit a negligible influence on the coordination number at the critical state, as demonstrated in Figure 7a,b.

In contrast, Figure 7c,d reveal that the coordination number is significantly influenced by C_c and C_s. The samples with higher C_c values tend to have larger coordination numbers, indicating a more interconnected contact network. Conversely, the samples with lower C_s values show a similar trend, reinforcing the role of size span in influencing particle

contacts. This finding suggests that a wider size span may increase the proportion of floating particles—those with insufficient contacts to contribute to stress transmission—thereby reducing the overall coordination number.
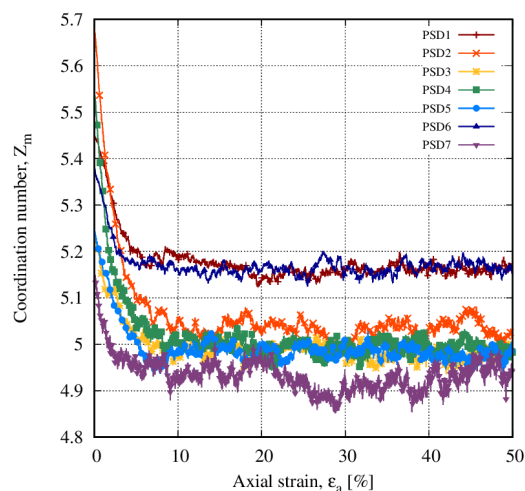

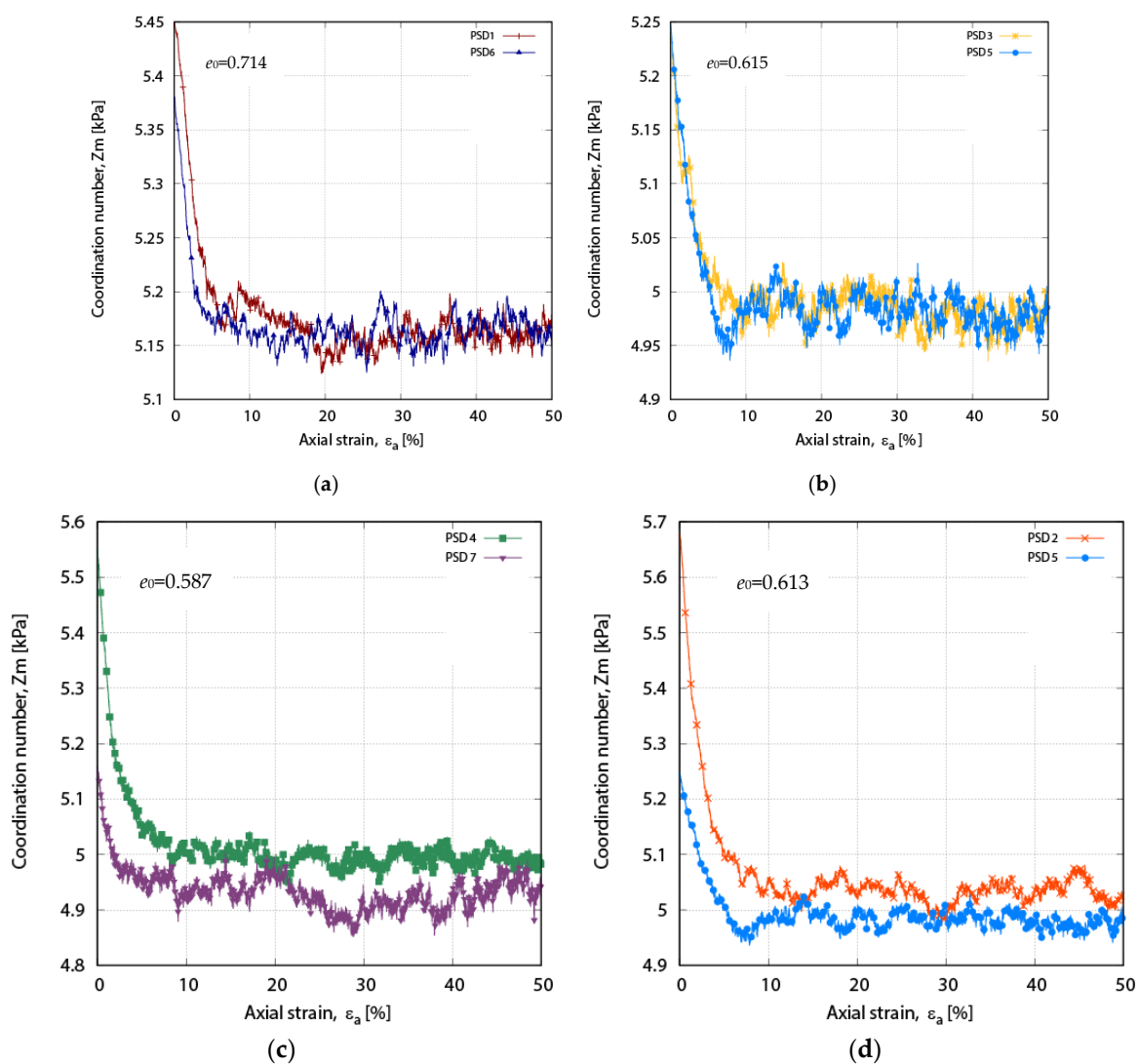**Figure 6.** Coordination number responses with various PSDs at $p_0' = 500$ kPa.

Figure 7. Effect of descriptors on the evolution of coordination number: (**a**) D_{50} effect; (**b**) C_u effect; (**c**) C_c effect; (**d**) C_s effect.

In addition to the coordination number, the internal structure, or fabric, of granular soils is also investigated. The fabric of granular materials refers to the collective microstructural features within the Representative Elemental Volume (REV), including the spatial arrangement of grains, the distribution of voids, and the interactions between particles [45].

In this study, a contact normal vector-based deviatoric second-order fabric tensor **F** is used to characterize the microstructure of the granular assemblies. This approach is derived from Kanatani's equation [46] where $f(\mathbf{n})$ is the density function that defines the distribution of contact normals. The fabric tensor **G** is the symmetric second-order tensor, and **F** represents its deviatoric part. The mathematical formulation is as follows:

$$G_{ij} = \int_n f(\boldsymbol{n}) n_i n_j dn \tag{12}$$

$$f(n) = \frac{1}{4\pi} \left(1 + F_{ij} n_i n_j \right) \tag{13}$$

$$F_{ij} = \frac{15}{2} \left(G_{ij} - \frac{1}{3} \delta_{ij} \right) \tag{14}$$

$$F = \sqrt{F_{ij} : F_{ij}} \tag{15}$$

Following Yang and Wu [47], this deviatoric fabric tensor is normalized by dividing by the volume, such that $F' = \frac{F}{v} = \frac{F}{1+e}$, where e is the void ratio. As previously mentioned, **F** has two invariants: the norm F and unit direction $\mathbf{n}_F$. The direction $\mathbf{n}_F$ is related to the Lode angle of the fabric, θ_F, through the expression $\cos 3\theta_F = \sqrt{6} \mathrm{tr} \mathbf{n}_F^3$.

The evolution of the fabric tensor during shearing was examined for all the PSDs. Figure 8 shows that the fabric norm increases with the axial strain for all samples, regardless of the PSD. Although the rate of fabric evolution varies, all the samples eventually reach a similar fabric value at the critical state. Regarding the fabric direction, a significant reduction in the fabric Lode angles is observed at the very beginning of shearing (less than 2–3% axial strain), which occurs much more rapidly than the evolution of the fabric norm (which takes approximately 30–50% of the axial strain). Figure 9 demonstrates that the fabric Lode angles eventually drop to zero, accompanied by slight fluctuations, indicating that the fabric direction quickly aligns with the loading direction.
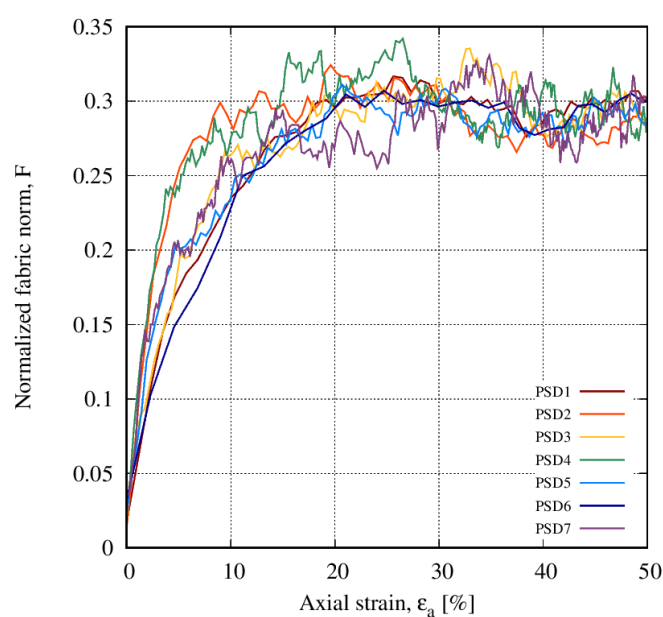

Figure 8. Fabric evolution of samples with various PSDs.
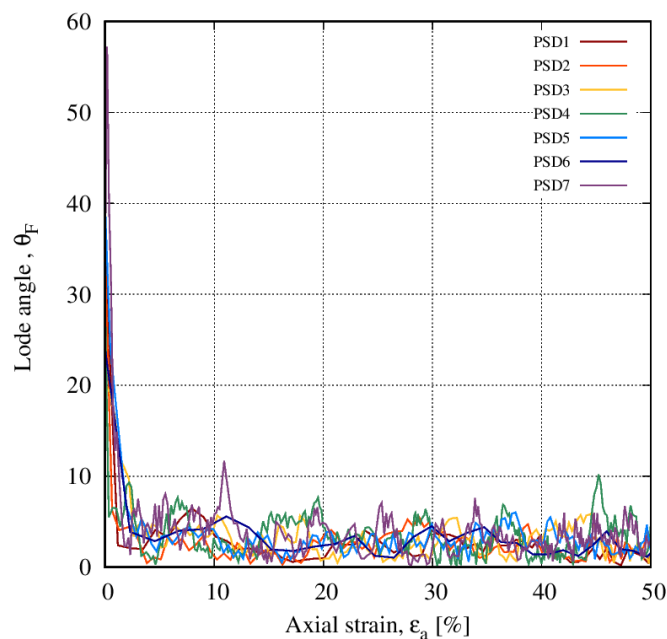
Figure 9. Lode angle evolution of samples with various PSDs.

3.3. Critical State Responses

As mentioned before, three planes are usually studied under anisotropic critical state theory, which are the p'-q plane, e-p' plane, and fabric space. In this study, all the critical stress states obtained for the different PSDs are shown in the p'-q plane in Figure 10. It can be concluded that all samples exhibit a unique critical stress ratio $M_c \approx 0.77$, which is consistent with previous Discrete Element Method (DEM) results [48–50]. The data from all samples can be fitted by a single straight line, suggesting that none of the PSD shape descriptors are correlated with the critical state strength.
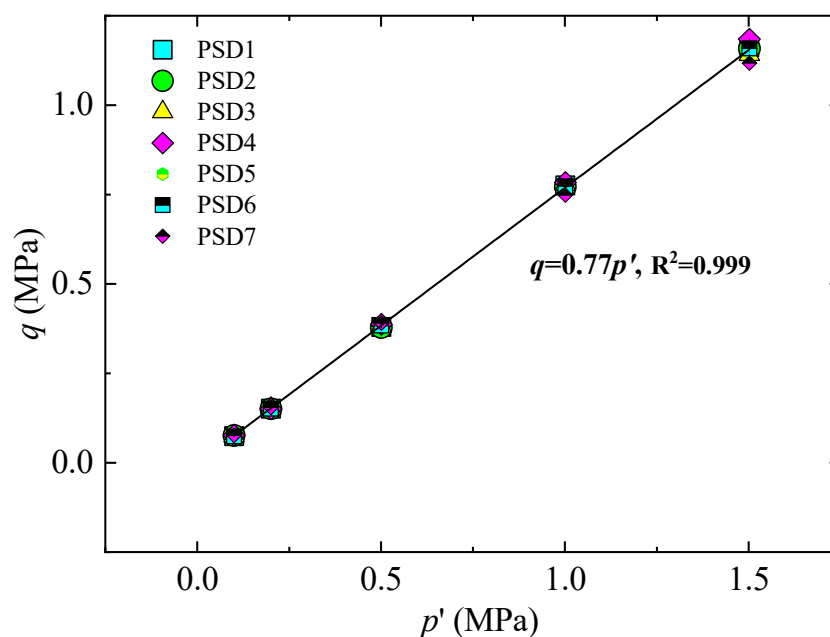
Figure 10. Critical states in p'-q plane of all samples.

Figure 11a illustrates the relationship between the critical state void ratio and mean effective stress in a logarithmic coordinate system. It can be observed that the location of the critical state line (CSL) in the *e-logp'* plane varies with the PSD shape. Specifically, both

higher C_s and lower C_c lead to a lower CSL position. In general, it can be stated that a wider PSD results in a lower CSL location. Interestingly, although the PSDs of samples 3 and 5 differ due to variations in C_u, their CSLs coincide. Similarly, the CSLs of parallel PSDs (PSD1 and PSD6) appear to overlap.
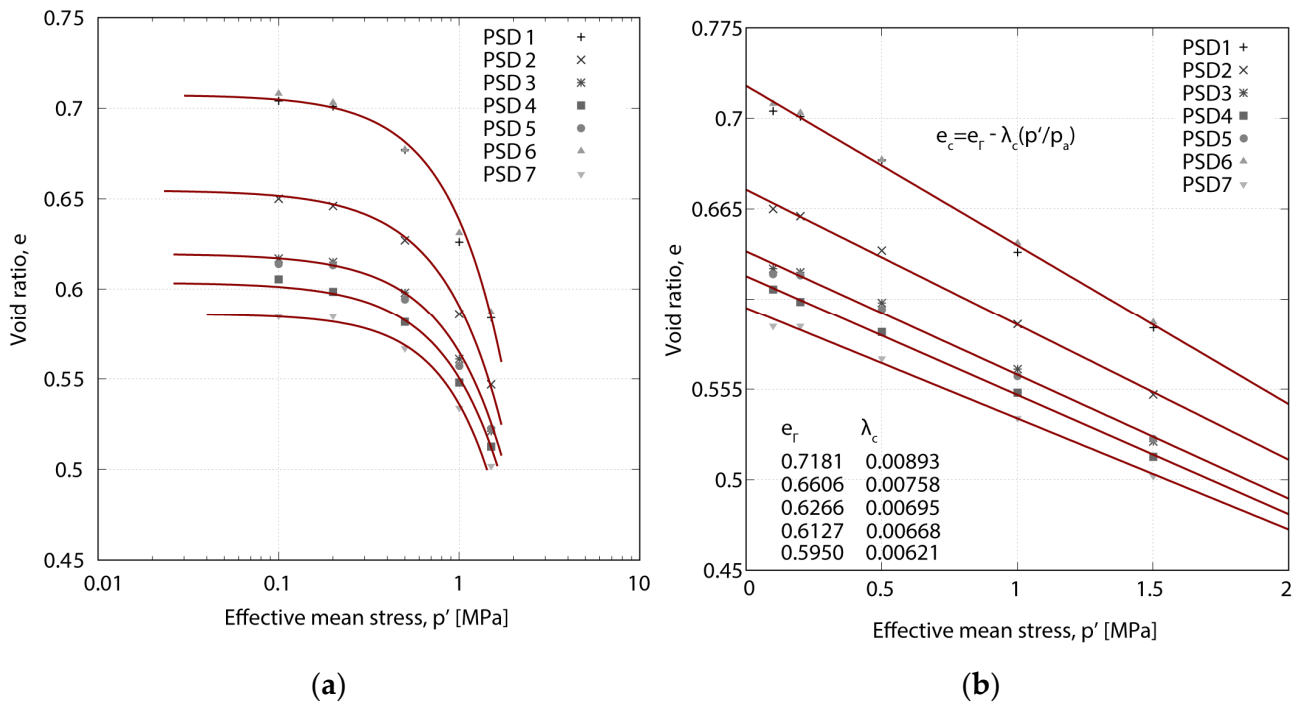
Figure 11. Critical states void ratio: (**a**) *e-logp′* plane; (**b**) *e-p′* plane.

To investigate this further, the critical state lines for non-cohesive soils are straightened in the $e^{-} - (p'/p_a)^{\xi}$ plane by use of the approach by Li and Wang's approach [51], as expressed in Equation (16):

$$e_c = e_\Gamma - \lambda_c (p'/p_a)^{\xi} \tag{16}$$

where p_a is the atmospheric pressure (101.325 kPa), e_Γ is the intersection of the CSL on the e-axis, λ_c is the slope of the CSL, and ξ is a constant parameter used for fine-tuning. As noted by [52], ξ is not a sensitive parameter and is set to 1.0 for simplicity.

Figure 11b shows the results of the seven PSDs grouped into five categories. In general, a wider PSD (with larger C_u or C_s) corresponds to a lower CSL position. The slopes of the CSLs also vary within a narrow range. Thus, the positional changes of the CSL due to PSD variations can be described by two main components: a downward translational shift and a counterclockwise rotational shift. These two shifting modes are consistent with previous experimental findings. It appears that C_c moves the CSL downward with negligible rotation, while C_s causes both a downward movement and a counterclockwis rotation.

Figure 12 further illustrates the effect of PSD descriptors on the critical state void ratio, e_c. It is evident that D_{50} and C_u have no significant effect on the critical state void ratio. However, Figure 12c,d show that the CSL for samples with higher C_c and lower C_s is positioned higher in the *e-p′* plane. Interestingly, the intersection of the CSL seems to be related to the coordination number. As shown in Figure 13, as the e_Γ increases, the coordination number at the critical state also increases.
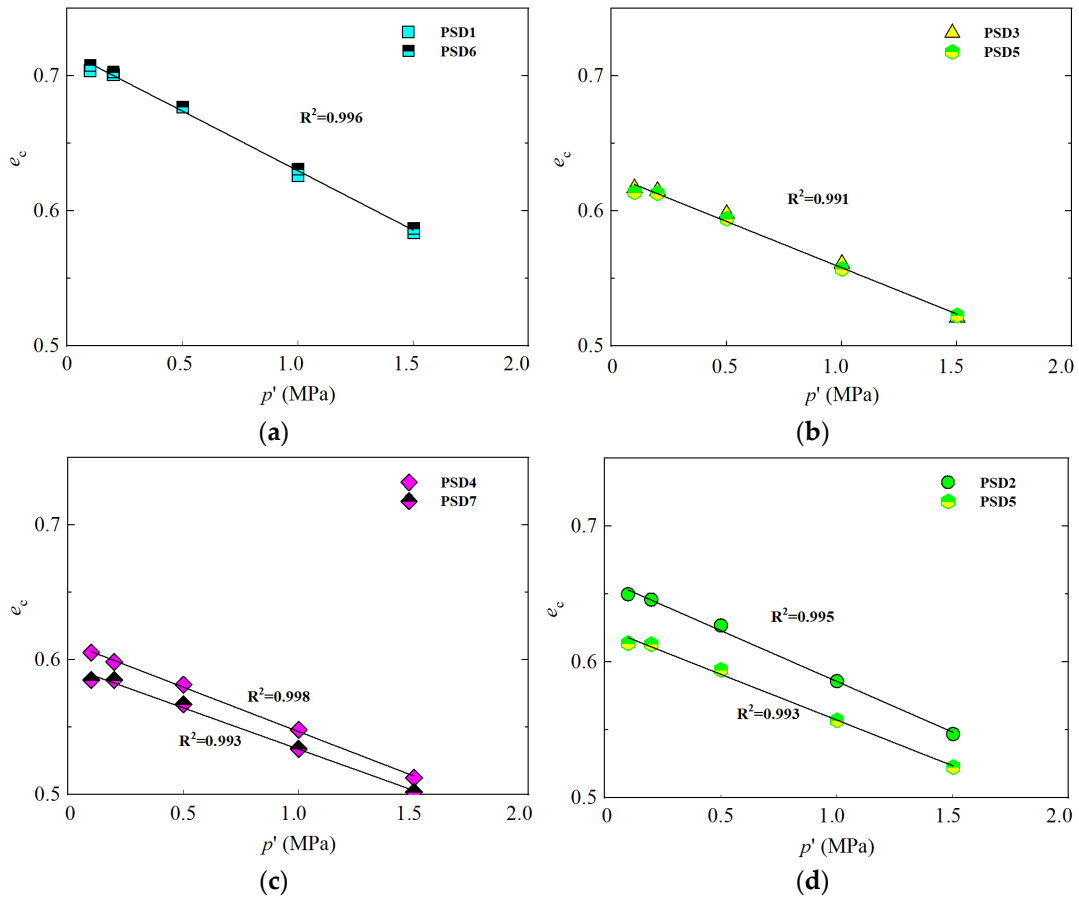
Figure 12. Effect of descriptors on critical state void ratio: (**a**) D_{50} effect; (**b**) C_u effect; (**c**) C_c effect; (**d**) C_s effect.
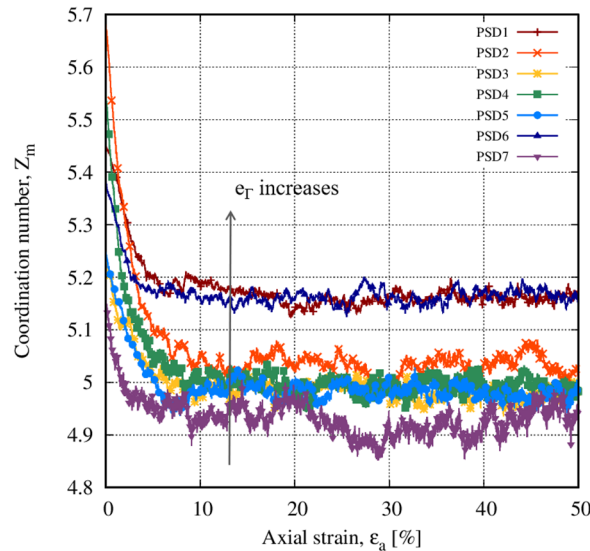
Figure 13. Critical state coordination number relationship with e_Γ.

Figure 14 presents the critical values of F'_c from simulations conducted with seven different PSDs. The coefficient of variation (CoV) is used to quantify the degree of deviation of the fabric norm from its mean value. Overall, the critical fabric norm is found to be a unique value, $F'_c = 0.293$. This suggests that the critical state fabric norm is independent of both the critical void ratio e_c and the mean effective stress p', which is consistent with the anisotropic critical state theory.
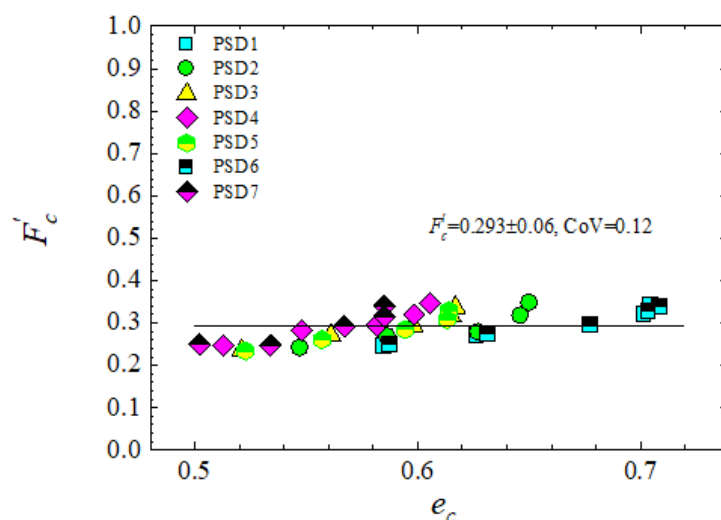
Figure 14. Critical state fabric norm.

4. Discussion and Conclusions

Although the effect of the PSD shape on the critical state behavior of granular materials has been widely studied, particularly concerning the coefficient of uniformity (C_u), the relationship between the PSD shape and the location of the critical state line (CSL) remains unclear. This paper expands on previous studies by considering four PSD shape descriptors—the mean particle size (D_{50}), coefficient of uniformity (C_u), coefficient of uniformity (C_c), and coefficient of uniformity (C_s). A series of systematic 3D-DEM simulations was conducted to analyze the effects of these different PSD shape descriptors on the mechanical behavior of granular materials. Seven distinct PSDs were carefully designed so that the influence of each descriptor could be investigated separately. Particular emphasis was placed on critical state behavior, interpreted within the framework of anisotropic critical state theory (ACST). A series of constant-mean effective stress drained triaxial tests were performed, and the critical state behavior was examined on both the macroscopic and microscopic scales in terms of the critical stress ratio, critical state void ratio, and critical state fabric norm. According to the simulation results, the following conclusions can be drawn:

1. Isolation of the effect of PSD shape descriptors:

The DEM numerical strategy employed in this study allows for the isolation of the effects of PSD shape descriptors on the mechanical behavior of a granular assembly. It was found that not all descriptors significantly impact the mechanical responses. Specifically, D_{50} and C_u had little to no effect on most of the mechanical properties, including the deviatoric stress, volumetric strain, and coordination number. Note that the simulations shown here are performed by use of periodic boundaries (free from boundary effects); hence, the effect of D_{50} is not expected; however, it is clear from the results presented that the increased particle masses resulting from scaling up the PSD have a slight effect. However, both C_c, and C_s had a significant impact on the macroscopic mechanical properties, microscopic responses, and critical state properties. This also emphasizes the need to accurately describe the PSD. In some cases, it may be necessary to use alternative PSD descriptors (such as when gap-graded soils or soils with a significant amount of fines are considered).

2. Critical state strength and void ratio:

The critical state strength appears to be insensitive to the PSD shape descriptors considered in this study. In contrast, the critical state void ratio was significantly affected by the PSD shape. Generally, a wider PSD (with higher C_u and C_s values) results in a lower

CSL position in the e-p' plane. While both C_u and C_s represent the range of particle sizes, C_s significantly affects the CSL position, while C_u has a minimal effect.

3. CSL Shifting Modes:

Two distinct shifting modes of the CSL in the e-p' plane were observed: downward translational shifts and counterclockwise rotational shifts. An increase in C_s caused both a downward movement and counterclockwise rotation of the CSL. In contrast, a decrease in C_c resulted in a downward shift with negligible rotation.

4. Coordination Number and CSL Intersection:

The intersection of CSL appears to be related to the coordination number. As the e_Γ increases, the coordination number at the critical state also increases. Moreover, the coordination number stabilizes at relatively small strain levels (<10%), while the fabric continues to evolve towards the critical state.

5. Microstructure Evolution:

The evolution of the microstructure is quantified using the deviatoric fabric tensor, which captures both the direction and norm of the fabric. The fabric direction evolves towards the loading direction at the early stages of shearing. The fabric norm evolves more slowly and appears to reach a unique value for all seven PSDs. The critical state fabric norm is independent of both the critical void ratio and the mean effective stress. Furthermore, while the critical fabric norm is generally consistent across materials, samples with different PSDs tend to converge on the same value for the critical state fabric norm.

This study demonstrates that the PSD shape parameters have distinct effects in the two critical state spaces. On the one hand, the stress ratio at the critical state is shown to be independent of the PSD. While previous research has suggested similar findings, it has primarily considered C_u alone. This study extends the validity of these results by showing that the critical state shear strength is independent not only of C_u, but also of D_{50}, C_u, and C_c. Thus, we can confidently state that there is no relationship between the PSD and critical state shear strength.

On the other hand, the simulation results highlight that the critical state void ratio is significantly affected by the PSD shape. Notably, C_u has no impact on the dilatancy or critical state void ratio, which contrasts with some previous studies. This discrepancy may arise from those studies considering only C_u and not controlling for other PSD shape descriptors, such as C_c and C_s, which were found to be the main factors influencing both the macroscopic and microscopic responses in this study. It appears that the pattern of these responses cannot be captured by any single descriptor. Therefore, a more comprehensive description of the PSD needs to be developed.

These numerical findings may offer valuable insights for developing constitutive models of sand that undergo grading variations, such as those caused by crushing and erosion, and for addressing fractal problems related to micro-mechanics in soils.

Author Contributions: Conceptualization, M.J. and D.B.; investigation, K.Y.; methodology, M.J. and D.B.; resources, Z.D.; validation, M.J. and D.B.; writing—original draft, M.J.; writing—review and editing, D.B., Z.D. and K.Y. All authors have read and agreed to the published version of the manuscript.

Data Availability Statement: All the data will be provided under reasonable request.

Conflicts of Interest: The authors declare no conflicts of interest.

References

1. Kuang, D.; Long, Z.; Wang, J.; Zhou, X.; Yu, P. Experimental Study on Particle Size Effect on Mechanical Behaviour of Dense Calcareous Sand. *Soils Rocks* **2020**, *43*, 567–574. [CrossRef]
2. Rezvani, R.; Nabizadeh, A.; Amin Tutunchian, M. The Effect of Particle Size Distribution on Shearing Response and Particle Breakage of Two Different Calcareous Soils. *Eur. Phys. J. Plus* **2021**, *136*, 1008. [CrossRef]
3. Chen, C.; Zhang, X.; Sun, Y.; Zhang, L.; Rui, R.; Wang, Z. Discrete Element Modelling of Fractal Behavior of Particle Size Distribution and Breakage of Ballast under Monotonic Loading. *Fractal Fract.* **2022**, *6*, 382. [CrossRef]
4. Shi, X.; Xu, J.; Guo, N.; Bian, X.; Zeng, Y. A Novel Approach for Describing Gradation Curves of Rockfill Materials Based on the Mixture Concept. *Comput. Geotech.* **2025**, *177*, 106911. [CrossRef]
5. Shi, X.; He, Z.; Zhao, J.; Liu, J. Determination of the Size of Representative Volume Element for Gap-Graded Granular Materials. *Powder Technol.* **2024**, *437*, 119578. [CrossRef]
6. Li, K.; Yang, H.; Han, X.; Xue, L.; Lv, Y.; Li, J.; Fu, Z.; Li, C.; Shen, W.; Guo, H.; et al. Fractal Features of Soil Particle Size Distributions and Their Potential as an Indicator of Robinia Pseudoacacia Invasion1. *Sci. Rep.* **2018**, *8*, 7075. [CrossRef] [PubMed]
7. Mohammad Mahdi, C.; Dahmardeh Ghaleno, M.R. Evaluating Fractal Dimension of the Soil Particle Size Distributions and Soil Water Retention Curve Obtained from Soil Texture Components. *Arch. Agron. Soil Sci.* **2020**, *66*, 1668–1678. [CrossRef]
8. Bai, Y.; Qin, Y.; Lu, X.; Zhang, J.; Chen, G.; Li, X. Fractal Dimension of Particle-Size Distribution and Their Relationships with Alkalinity Properties of Soils in the Western Songnen Plain, China. *Sci. Rep.* **2020**, *10*, 20603. [CrossRef] [PubMed]
9. He, S.-H.; Ding, Z.; Hu, H.-B.; Gao, M. Effect of Grain Size on Microscopic Pore Structure and Fractal Characteristics of Carbonate-Based Sand and Silicate-Based Sand. *Fractal Fract.* **2021**, *5*, 152. [CrossRef]
10. Shen, X.; Shen, Y.; Xu, J.; Liu, H. Influence of the Fractal Distribution of Particle Size on the Critical State Characteristics of Calcareous Sand. *Fractal Fract.* **2022**, *6*, 165. [CrossRef]
11. Monkul, M.M.; Etminan, E.; Şenol, A. Influence of Coefficient of Uniformity and Base Sand Gradation on Static Liquefaction of Loose Sands with Silt. *Soil Dyn. Earthq. Eng.* **2016**, *89*, 185–197. [CrossRef]
12. Danesh, A.; Palassi, M.; Mirghasemi, A.A. Effect of Sand and Clay Fouling on the Shear Strength of Railway Ballast for Different Ballast Gradations. *Granul. Matter* **2018**, *20*, 51. [CrossRef]
13. Monkul, M.M.; Kendir, S.B.; Tütüncü, Y.E. Combined Effect of Fines Content and Uniformity Coefficient on Cyclic Liquefaction Resistance of Silty Sands. *Soil Dyn. Earthq. Eng.* **2021**, *151*, 106999. [CrossRef]
14. Rasti, A.; Adarmanabadi, H.R.; Pineda, M.; Reinikainen, J. Evaluating the Effect of Soil Particle Characterization on Internal Friction Angle. *Am. J. Appl. Sci.* **2021**, *14*, 129–138. [CrossRef]
15. Banerjee, S.K.; Yang, M.; Taiebat, M. Effect of Coefficient of Uniformity on Cyclic Liquefaction Resistance of Granular Materials. *Comput. Geotech.* **2023**, *155*, 105232. [CrossRef]
16. Wei, Y.; Yang, Y.; Tao, M. Effects of Gravel Content and Particle Size on Abrasivity of Sandy Gravel Mixtures. *Eng. Geol.* **2018**, *243*, 26–35. [CrossRef]
17. Onyelowe, K.C.; Shakeri, J. Intelligent Prediction of Coefficients of Curvature and Uniformity of Hybrid Cement Modified Unsaturated Soil with NQF Inclusion. *Clean. Eng. Technol.* **2021**, *4*, 100152. [CrossRef]
18. Khater, S. Development of Soil Particle Size Distribution Model and Determination of All Related Coefficients. *Ann. Agric. Sci. Moshtohor* **2023**, *61*, 269–278. [CrossRef]
19. Azéma, E.; Linero, S.; Estrada, N.; Lizcano, A. Shear Strength and Microstructure of Polydisperse Packings: The Effect of Size Span and Shape of Particle Size Distribution. *Phys. Rev. E* **2017**, *96*, 022902. [CrossRef] [PubMed]
20. Roscoe, K.H.; Schofield, A.N.; Wroth, C.P. On The Yielding of Soils. *Géotechnique* **1958**, *8*, 22–53. [CrossRef]
21. Bandini, V.; Coop, M.R. The Influence of Particle Breakage on the Location of the Critical State Line of Sands. *Soils Found.* **2011**, *51*, 591–600. [CrossRef]
22. Xiao, Y.; Liu, H.; Ding, X.; Chen, Y.; Jiang, J.; Zhang, W. Influence of Particle Breakage on Critical State Line of Rockfill Material. *Int. J. Geomech.* **2016**, *16*, 04015031. [CrossRef]
23. Guo, W.-L.; Cai, Z.-Y.; Wu, Y.-L.; Geng, Z.-Z. Estimations of Three Characteristic Stress Ratios for Rockfill Material Considering Particle Breakage. *Acta Mech. Solida Sin.* **2019**, *32*, 215–229. [CrossRef]
24. Yan, W.M.; Dong, J. Effect of Particle Grading on the Response of an Idealized Granular Assemblage. *Int. J. Geomech.* **2011**, *11*, 276–285. [CrossRef]
25. Yang, J.; Luo, X.D. The Critical State Friction Angle of Granular Materials: Does It Depend on Grading? *Acta Geotech.* **2018**, *13*, 535–547. [CrossRef]
26. Li, G.; Ovalle, C.; Dano, C.; Hicher, P.-Y. Influence of Grain Size Distribution on Critical State of Granular Materials. In *Constitutive Modeling of Geomaterials*; Yang, Q., Zhang, J.-M., Zheng, H., Yao, Y., Eds.; Springer Series in Geomechanics and Geoengineering; Springer: Berlin/Heidelberg, Germany, 2013; pp. 207–210. ISBN 978-3-642-32813-8.
27. Thevanayagam, S.; Shenthan, T.; Mohan, S.; Liang, J. Undrained Fragility of Clean Sands, Silty Sands, and Sandy Silts. *J. Geotech. Geoenviron. Eng.* **2002**, *128*, 849–859. [CrossRef]

28. Murthy, T.G.; Loukidis, D.; Carraro, J.A.H.; Prezzi, M.; Salgado, R. Undrained Monotonic Response of Clean and Silty Sands. *Géotechnique* **2007**, *57*, 273–288. [CrossRef]

29. Carrera, A.; Coop, M.; Lancellotta, R. Influence of Grading on the Mechanical Behaviour of Stava Tailings. *Géotechnique* **2011**, *61*, 935–946. [CrossRef]

30. Cundall, P.A.; Strack, O.D.L. A Discrete Numerical Model for Granular Assemblies. *Géotechnique* **1979**, *29*, 47–65. [CrossRef]

31. Muir Wood, D. *Soil Behaviour and Critical State Soil Mechanics*; Cambridge University Press: Cambridge, UK; New York, NY, USA, 1990; ISBN 978-0-521-33249-1.

32. Li, X.S.; Dafalias, Y.F. Anisotropic Critical State Theory: Role of Fabric. *J. Eng. Mech.* **2012**, *138*, 263–275. [CrossRef]

33. Dafalias, Y.F.; Taiebat, M. SANISAND-Z: Zero Elastic Range Sand Plasticity Model. *Géotechnique* **2016**, *66*, 999–1013. [CrossRef]

34. Mo, W.; Wang, R.; Zhang, J.; Dafalias, Y.F. Quantification of Fabric Evolution in Granular Material under Cyclic Loading. *Int. J. Numer. Anal. Methods Geomech.* **2024**, *48*, 701–726. [CrossRef]

35. Li, X.; Li, X.-S. Micro-Macro Quantification of the Internal Structure of Granular Materials. *J. Eng. Mech.* **2009**, *135*, 641–656. [CrossRef]

36. Yang, Z.X.; Li, X.S.; Yang, J. Quantifying and Modelling Fabric Anisotropy of Granular Soils. *Géotechnique* **2008**, *58*, 237–248. [CrossRef]

37. Wu, Q.X.; Yang, Z.X.; Li, X. Numerical Simulations of Granular Material Behavior under Rotation of Principal Stresses: Micromechanical Observation and Energy Consideration. *Meccanica* **2019**, *54*, 723–740. [CrossRef]

38. Li, X.S.; Dafalias, Y.F. Dissipation Consistent Fabric Tensor Definition from DEM to Continuum for Granular Media. *J. Mech. Phys. Solids* **2015**, *78*, 141–153. [CrossRef]

39. Zhao, J.; Guo, N. A New Definition on Critical State of Granular Media Accounting for Fabric Anisotropy. *AIP Conf. Proc.* **2013**, *1542*, 229–232.

40. Liu, J.; Zhou, W.; Ma, G.; Yang, S.; Chang, X. Strong Contacts, Connectivity and Fabric Anisotropy in Granular Materials: A 3D Perspective. *Powder Technol.* **2020**, *366*, 747–760. [CrossRef]

41. Xu, M.Q.; Pan, K.; Duan, B.; Wu, Q.X.; Yang, Z.X. Investigating the Influence of Particle Shape on Discrete Element Modeling of Granular Soil under Multidirectional Cyclic Shearing. *Soil Dyn. Earthq. Eng.* **2025**, *189*, 109097. [CrossRef]

42. Kozicki, J.; Donzé, F.V. A New Open-Source Software Developed for Numerical Simulations Using Discrete Modeling Methods. *Comput. Methods Appl. Mech. Eng.* **2008**, *197*, 4429–4443. [CrossRef]

43. Thornton, C. Numerical Simulations of Deviatoric Shear Deformation of Granular Media. *Géotechnique* **2000**, *50*, 43–53. [CrossRef]

44. Thornton, C.; Zhang, L. On the Evolution of Stress and Microstructure during General 3D Deviatoric Straining of Granular Media. *Géotechnique* **2010**, *60*, 333–341. [CrossRef]

45. Oda, M.; Nakayama, H. Introduction of Inherent Anisotropy of Soils in the Yield Function. In *Studies in Applied Mechanics*; Elsevier: Amsterdam, The Netherlands, 1988; Volume 20, pp. 81–90. ISBN 978-0-444-70523-5.

46. Ken-Ichi, K. Distribution of Directional Data and Fabric Tensors. *Int. J. Eng. Sci.* **1984**, *22*, 149–164. [CrossRef]

47. Yang, Z.X.; Wu, Y. Critical State for Anisotropic Granular Materials: A Discrete Element Perspective. *Int. J. Geomech.* **2017**, *17*, 04016054. [CrossRef]

48. Kuhn, M.R. The Critical State of Granular Media: Convergence, Stationarity and Disorder. *Géotechnique* **2016**, *66*, 902–909. [CrossRef]

49. Kodicherla, S.P.K.; Gong, G.; Wilkinson, S. Exploring the Relationship between Particle Shape and Critical State Parameters for Granular Materials Using DEM. *SN Appl. Sci.* **2020**, *2*, 2128. [CrossRef]

50. Zhu, M.; Gong, G.; Xia, J.; Wilkinson, S. DEM Investigation of Strength and Critical State Behaviours of Granular Materials under True Triaxial Loadings. *Particuology* **2024**, *85*, 198–212. [CrossRef]

51. Li, X.S.; Wang, Y. Linear Representation of Steady-State Line for Sand. *J. Geotech. Geoenviron. Eng.* **1998**, *124*, 1215–1217. [CrossRef]

52. Li, X.; Yu, H.; Li, X. A Virtual Experiment Technique on the Elementary Behaviour of Granular Materials with Discrete Element Method. *Int. J. Numer. Anal. Methods Geomech.* **2013**, *37*, 75–96. [CrossRef]